

Supporting Information

Double bond characterization of free fatty acids directly from biological tissues by ultraviolet photodissociation

Clara L. Feider[†], Luis A. Macias[†], Jennifer S. Brodbelt, Livia S. Eberlin*

Department of Chemistry, The University of Texas at Austin, Austin, TX, 78712

[†]equal contribution

*to whom correspondence may be addressed: liviase@utexas.edu

Table of Contents

Supplementary methods

Strategy for determination of interfering fragments during DESI-MS imaging experiments

Supporting Table S1: Structures and molecular weights of fatty acids used in this study

Supporting Table S2: Structures, molecular weights, and synthetic reagents used to synthesize all dicationic compounds used in this study

Supporting Table S3: FA-DC complexes detected from ovarian tissue

Supporting Table S4: Hypothetical diagnostic fragment peaks for FA 18:2 isomers

Supporting Table S5: Hypothetical diagnostic fragment peaks for FA 20:4 isomers

Supporting Table S6: Breast biopsy patient demographics

Supporting Figure S1: FA 18:1 (11Z) complexed with multiple dication species

Supporting Figure S2: HCD fragmentation spectrum of the 1,8-ethyl dication

Supporting Figure S3: DESI-UVPD-MS spectrum from background signal of the DESI spray solvent on the glass slide

Supporting Figure S4: UVPD of free 18:1 FA in the negative ion mode

Supporting Figure S5: UVPD of free 18:2 FA in the negative ion mode

Supporting Figure S6: MS1 spectrum of FA 18:1 complexed to 1,3-ethyl dication

Supporting Figure S7: HCD of FA 18:1 (9Z) – DC complex

Supporting Figure S8: Full DESI-MS spectrum of mouse brain with and without DC

Supporting Figure S9: Full UVPD MS spectrum of FA 18:2

Supporting Figure S10: Expanded view of UVPD 18:2 spectrum

Supporting Figure S11: DESI-UVPD MS imaging of FA 18:2 from an ovarian tumor tissue

Supporting Figure S12: Full UVPD MS spectrum of FA 20:4

Supporting Figure S13: Expanded view of UVPD 20:4 spectrum

Supporting Figure S14: DESI-UVPD MS imaging of FA 20:4 from an ovarian tumor tissue

Supporting Figure S15: ESI and DESI comparisons of fragment abundances

Supporting Figure S16: Evaluation of interfering internal fragment ion at m/z 505.47

Supporting Figure S17: ESI-UVPD relative quantification of DC•FA 18:1 isomers

Supporting Figure S18: Calibration curves for DESI-UVPD MS of 9Z and 11Z FA isomers

Supporting Figure S19: All DESI-UVPD MS images from PR- and PR+ samples.

Supplementary references

Supplementary methods:

Chemicals

FA standards were purchased from Sigma-Aldrich (St. Louis, MO) and used without further purification. The structures and molecular weights of all fatty acids included in this study are listed in **Table S1**. HPLC-grade methanol for ESI infusion of FAs was purchased from EMD Millipore (Billerica, MA). All chemicals for the synthesis of the stable DC compounds, including 1,6-dibromohexane, 1,8-dibromooctane, 1-methylpyrrolidine, 1-ethylpyrrolidine, ethyl acetate, isopropyl alcohol, and phosphorus pentoxide were purchased from Sigma Aldrich (Milwaukee, WI). High purity methanol and acetone used for DESI-MS imaging was purchased from Fisher Scientific (Hampton, NH).

Synthesis and evaluation of dicationic compounds

Four DCs, displayed in **Table S2**, were synthesized following established procedures reported in the literature.¹⁻³ These DCs were selected to mitigate potentially confounding photodissociation channels and spectral complexity. Briefly, pyrrolidine compounds were combined with brominated carbon chain compounds in a 2:1 molar ratio and dissolved in 10 mL of isopropanol and stirred under reflux at 95°C for 24 hr. The isopropanol was then evaporated under vacuum and the remaining salt was dissolved in 10ml of water and extracted three times with ethyl acetate. The aqueous layer was collected, and the solvent was evaporated under vacuum. The remaining product was dried in a desiccator with P₂O₅ prior to solvation with the MS solvent for experiments. All possible combinations of 1,6-dibromohexane, 1,8-dibromooctane, 1-methylpyrrolidine, and 1-ethylpyrrolidine were used to produce the four compounds under the same synthetic conditions. The four compounds were evaluated for efficient complexation with free FAs during DESI-MS analysis and for reduction of interfering fragment ions produced by UVPD. Due to a fragment ion produced from the 1-methylpyrrolidine containing compounds interfering with the distal diagnostic peak from the FA 18:1 (11Z) isomer (**Figure S1**), the 1-ethylpyrrolidine compounds were

Formatted: Not Highlight

selected as optimal for the present application. The synthetic yield of $C_8(\text{epy})_2\text{-Br}$, termed 1,8-ethyl DC, was greatest and thus utilized for all experiments described in this work. A tandem MS spectrum of this compound has been provided as **Figure S2** to illustrate successful synthesis of the proposed compound.

ESI-MS-UVPD Analysis

For direct infusion experiments, samples were diluted in methanol to a final concentration of 20 μM for individual FAs. For relative quantitation of FA 18:1 isomers, the total FA concentration was held constant at 20 μM while the isomeric ratio was varied. Quantitative analysis of polyunsaturated fatty acids was not explored. DC-bound FA complexes were generated via ESI in the positive ion mode by doping 1,8-ethyl DC (5 μM) to the FA methanolic solution and using an ESI spray voltage of 2.5 kV, capillary temperature of 275°C, sheath gas of 1 (arbitrary units) and a flow rate of 10 $\mu\text{L}/\text{min}$. Mass spectra were collected at an AGC target of 5×10^5 , 1 $\mu\text{scan}/\text{scan}$, reduced-profile mode, at a resolution of 60k. FAs and DC•FA complexes were manually selected for quadrupole isolation for ESI experiments with a 1 m/z window. Each mass spectrum is an average of 50 scans.

Tissue samples

Optimization of parameters was performed using mouse brain tissue samples, purchased from BioIVT (Westbury, NY). Frozen human tissue samples were obtained from the Cooperative Human Tissue Network (CHTN) and Asterand Biosciences (Detroit, MI) under approved IRB protocols. Samples were stored in a -80C freezer until sectioned. Tissue samples were sectioned at 10 μm thick using a CryoStar NX50 cryostat (Thermo Scientific, Waltham, MA) and thaw mounted on glass slides. After sectioning, the glass slides were stored at -80C. Immediately prior to MS imaging, the glass slides were thawed and dried in a hood ventilator for ~15 min.

DESI-UVPD MS imaging

DESI-UVPD-MS imaging was performed in the positive ion mode for the selected ion with an isolation width of 1.5 m/z centered at the mass of interest and a resolving power of 30,000 at m/z 200. The maximum injection time was set to 1800 msec to obtain optimal signal-to-noise of fragment peaks. DESI-UVPD-MS imaging was performed in the positive ion mode with an isolation width of 1.5 m/z centered at the mass of interest and a resolving power of 30,000. Imaging data was acquired in full profile mode. The spatial resolution used for all DESI-MS imaging experiment presented in this work was 200 μm . Prior to DESI-UVPD-MS imaging of samples, the solvent system was used to analyze the surrounding area of the glass slide to ensure that the background presence of FA 18:1, which can occasionally be present within the DESI solvent spray or on glass surfaces, was negligible. An example spectrum from a DESI-UVPD-MS analysis of a blank glass slide has been provided as **Figure S3**, showing low abundance of the precursor at m/z 591.580 ($\text{NL}\approx 4\text{E}3$) in the background in a full MS tissue analysis in comparison to the abundance detected on tissue ($\text{NL}\approx 1\text{E}6$), and that there is no detectable signal for the diagnostic peaks of either isomer during DESI-UVPD MS analysis on a glass slide.

2D image processing

Thermo RAW files were converted to mzML files using msConvert (ProteoWizard) using a threshold peak filter of 50 to reduce file size.⁴ mzML files were then imported into R using the mzR package from Bioconductor repository. Images were constructed for each m/z value using the intensity of the exact m/z value ± 0.02 Da.

Data extraction and statistical analysis

After DESI-MS imaging of breast carcinoma tissues, the same sections analyzed were stained with hematoxylin and eosin (H&E) and evaluated by a pathologist for determination of regions of pure tumor tissue. Converted mzML files were then compiled into an imzML data format using

imzML converter⁵ and uploaded into MSiReader for extraction of the double bond diagnostic m/z peaks within areas of breast carcinoma tissue.⁶ Extracted data was then imported into R and the $9\Delta/11\Delta$ ratios for each pixel were calculated.

Nomenclature

FA structures are described by the number of carbon atoms, followed by a colon and the number of double bonds. Carbon positions are described relative to the carboxyl carbon (C1). If the position of the double bonds is known, it is indicated in parentheses following the number of double bonds. The double bond geometry is indicated by Z (for cis), E (for trans), or Δ (for unknown) following the double bond position. For example, FA 18:2(9Z,12Z) corresponds to a fatty acid composed of an 18-carbon chain with two double bonds between C9 and C10 and C12 and C13, both in a cis configuration. For ease of discussion, fragment ions arising from cleavage of C-C bonds adjacent to C=C double bonds are referred to as proximal (represented by Z_p , E_p , Δ_p) and distal (represented by Z_d , E_d , Δ_d) in reference to the C-C bond on the carboxyl- and methyl-end, respectively.

Strategy for determination of interfering fragments during DESI-MS imaging experiments

Fragmentation of polyunsaturated FA differed from monounsaturated FA in the relative abundance of proximal and distal peaks. Both diagnostic fragments from monounsaturated lipids and FAs have typically exhibited similar ion abundances within each pair, but both ESI and DESI-MS results from the fragmentation of polyunsaturated FA show unequal relative abundances of the proximal and distal fragment ions.⁷ For example, the $9\Delta_p$ fragment of m/z 453.44 is consistently more abundant than the $9\Delta_d$ fragment of m/z 477.44. As the ovarian tissue section is more molecularly complex than FA standards used in optimization experiments, there is a higher chance that interfering fragment ions from co-isolated species overlap with the diagnostic

fragment ions and alter their observed abundance. To evaluate if these differences in the relative abundances are due to interfering ions, the ratio of the proximal and distal fragment ions was calculated for both ESI-MS and DESI-MS modes for both FA 18:2 and FA 20:4 (**Figure S15**). The proximal:distal ratio for every double bond pair produced upon UVPD was consistent between ESI and DESI analysis, suggesting these altered ratios do not originate from interfering isobars but rather represent preferential cleavages across the FA chain or overlapping fragmentation pathways of the DC•FA complexes.

Table S1. Structures and molecular weights of fatty acids standards used in this study.

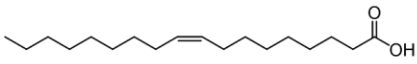
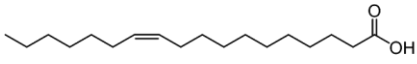
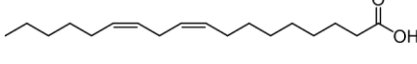
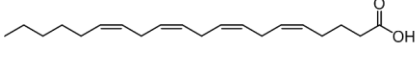
Lipid Name	Lipid Structure	Exact Mass (Da)
Oleic acid <i>cis</i> -9-Octadecenoic acid FA 18:1(9Z)		282.2559
<i>cis</i> -Vaccenic acid <i>cis</i> -11-Octadecenoic acid FA 18:1(11Z)		282.2559
Linoleic acid <i>cis</i> -9, <i>cis</i> -12-Octadecadienoic acid FA 18:2(9Z,12Z)		280.2402
Arachidonic acid <i>cis,cis,cis,cis</i> -5,8,11,14-Eicosatetraenoic acid 20:4(5Z,8Z,11Z,14Z)		304.2402

Table S2. Structures, molecular weights, and synthetic reagents used to synthesize all dicationic compounds used in this study.

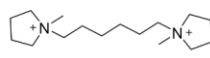
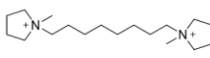
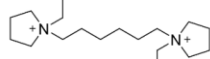
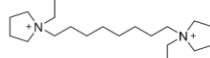
Molecule	Molecular Weight (g/mol)	Synthetic reagent A	Synthetic reagent B	Structure
$C_6(\text{mpy})_2\text{-Br}$	254.46	1,6-dibromohexane	1-methylpyrrolidine	
$C_8(\text{mpy})_2\text{-Br}$	282.52	1,8-dibromooctane	1-methylpyrrolidine	
$C_6(\text{epy})_2\text{-Br}$	282.52	1,6-dibromohexane	1-ethylpyrrolidine	
$C_8(\text{epy})_2\text{-Br}$	310.57	1,8-dibromooctane	1-ethylpyrrolidine	

Table S3. DC•FA complexes detected from ovarian tissue. Note that these assignments have been made on exact mass measurements alone.

Fatty Acid	Theoretical mass [M]	Observed mass (m/z) [M+DC] ⁺	Theoretical m/z [M+DC] ⁺	Mass error (ppm)
FA 16:1	254.2246	563.5503	563.551	-1.24
FA 16:0	256.2402	565.5657	565.5666	-1.59
FA 18:3	278.2246	587.5528	587.551	3.06
FA 18:2	280.2402	589.5669	589.5666	0.51
FA 18:1	282.2559	591.5812	591.5823	-1.86
FA 20:5	302.2246	611.5495	611.551	-2.45
FA 20:4	304.2402	613.5664	613.5666	-0.33
FA 20:3	306.2559	615.5795	615.5823	-4.55
FA 20:2	308.2715	617.5943	617.5979	-5.83
FA 20:1	310.2872	619.612	619.6136	-2.58
FA 22:6	328.2402	637.5661	637.5666	-0.78
FA 22:5	330.2559	639.5804	639.5823	-2.97
FA 22:4	332.2715	641.5967	641.5979	-1.87
FA 22:2	336.3028	645.6254	645.6292	-5.89
FA 22:1	338.3185	647.6444	647.6449	-0.77
FA 22:0	340.3341	649.6568	649.6605	-5.70

Table S4. Hypothetical diagnostic fragments that would result from UVPD of FA 18:2 isomers, compared to the peaks observed during UVPD analysis of the DC•FA 18:2 precursor. Observed *m/z* values suspected to be double bond diagnostic peaks have been included in the table, whereas “ - - ” has been added in place where no peak was observed at the theoretical *m/z* value. Note that these assignments have been made on exact mass measurements alone.

Fatty Acid	Hypothetical diagnostic fragment	Theoretical <i>m/z</i>	Observed <i>m/z</i>
18:2 (6 Δ ,9 Δ)	6 Δ _p	411.395	--
	6 Δ _d	435.395	435.392
	9 Δ _p	451.426	452.424
	9 Δ _d	475.426	--
18:2 (9 Δ ,12 Δ)	9 Δ _p	453.442	453.440
	9 Δ _d	477.442	477.440
	12 Δ _p	493.473	493.470
	12 Δ _d	517.473	517.470
18:2 (12 Δ ,15 Δ)	12 Δ _p	495.488	--
	12 Δ _d	519.488	--
	15 Δ _p	535.520	--
	15 Δ _d	559.520	559.516

Table S5. Hypothetical diagnostic fragments that would result from UVPD of FA 20:4 isomers, compared to the peaks observed during UVPD analysis of the DC•FA 20:4 precursor. Observed *m/z* values suspected to be double bond diagnostic peaks have been included in the table, whereas “ - - ” has been added in place where no peak was observed at the theoretical *m/z* value. Note that these assignments have been made on exact mass measurements alone.

Fatty Acid	Hypothetical diagnostic fragment	Theoretical <i>m/z</i>	Observed <i>m/z</i>
20:4 (5Δ, 8Δ, 11Δ, 14Δ)	5Δ _p	397.380	397.377
	5Δ _d	421.380	421.377
	8Δ _p	437.410	437.408
	8Δ _d	461.410	461.408
	11Δ _p	477.442	477.440
	11Δ _d	501.442	501.439
	14Δ _p	517.473	517.470
	14Δ _d	541.473	541.470
20:4 (8Δ, 11Δ, 14Δ, 17Δ)	8Δ _p	439.426	--
	8Δ _d	463.426	463.424
	11Δ _p	479.457	--
	11Δ _d	503.457	503.455
	14Δ _p	519.488	--
	14Δ _d	543.488	--
	17Δ _p	559.520	--
	17Δ _d	583.520	583.516

Table S6. Patient and sample demographics for breast cancer tissues. IDC = invasive ductal carcinoma, DCIS = ductal carcinoma in situ.

Sample	Patient Age	Patient Race	Gender	Histological subtype	Metastatic	ER	PR
1121412	41	White	Female	IDC	Yes	+	+
1162617	53	White	Female	IDC	No	+	+
1181239	57	Asian	Female	IDC	Yes	-	-
1170374F	67	White	Male	IDC	Yes	+	+
A144g	58	White	Female	DCIS	No	N/A	N/A
1085255F	50	Asian	Female	IDC	No	+	+
A054a	58	Black	Female	DCIS	No	N/A	N/A
A060h	68	White	Female	IDC	No	+	+
A074cc	42	White	Female	DCIS	No	N/A	N/A
A121g	36	Black	Female	DCIS	Yes	+	+
A177p	60	White	Female	IDC	Yes	-	-
A187a	58	White	Female	DCIS	No	N/A	N/A
A479c	69	White	Female	DCIS	No	+	-
ED76628	63	Asian	Female	IDC	Yes	-	+
ED77376	70	White	Female	IDC	No	+	+
ED79797	72	White	Female	IDC	Yes	+	+
M411101A18	55	Black	Female	IDC	No	-	-
M1170681	56	White	Female	IDC	Yes	+	+

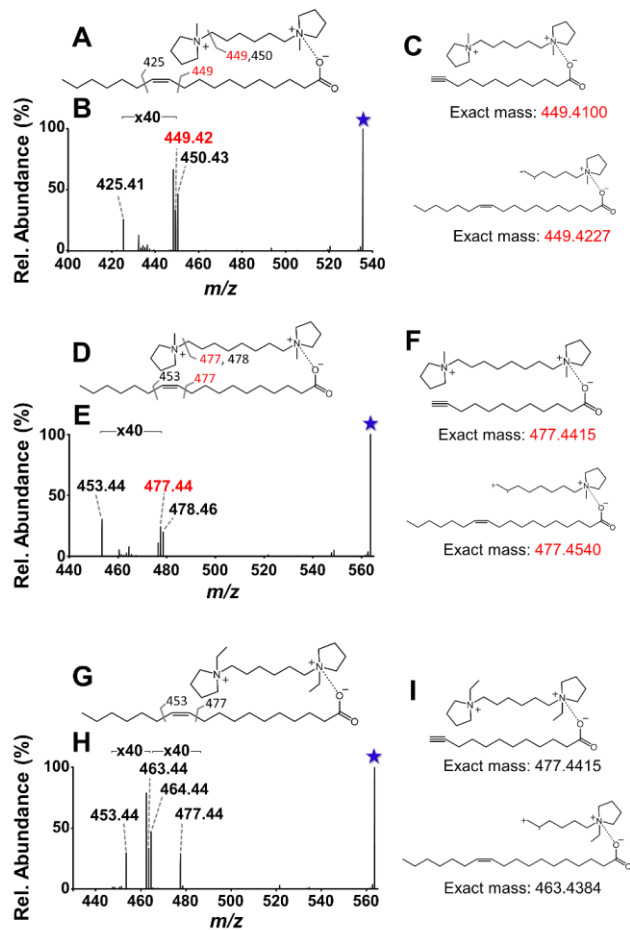


Figure S1. 193 nm UVPD (20 pulses, 4 mJ) mass spectra for FA 18:1(11Z) complexed to various dicationic compounds. Dications were selected to minimize the presence of isobaric UVPD fragments from the dicationic and FA structures. (A) Structure of 18:1(11Z) complexed to 1,6-methyl dication (m/z 535.52) with labelled fragments from corresponding (B) UVPD spectrum. (C) Isobaric fragment structures confounding interpretation are shown. (D) Structure of 18:1(11Z) complexed to 1,8-methyl dication (m/z 563.55) with labelled fragments from corresponding (E) UVPD spectrum. (F) Isobaric fragment structures confounding interpretation are shown. (G) Structure of 18:1(11Z) complexed to 1,6-ethyl (m/z 563.55) dication with labelled fragments from corresponding (H) UVPD spectrum. (I) Incorporation of an ethyl group on the quaternary amine results in separation of the confounding DC and FA fragment products in m/z space. Isobar signals and masses are highlighted in red font. Selected precursor ions are designated with a star. UVPD spectrum for 18:1(11Z) complexed to 1,8-ethyl dication is shown in **Figure 1C**.

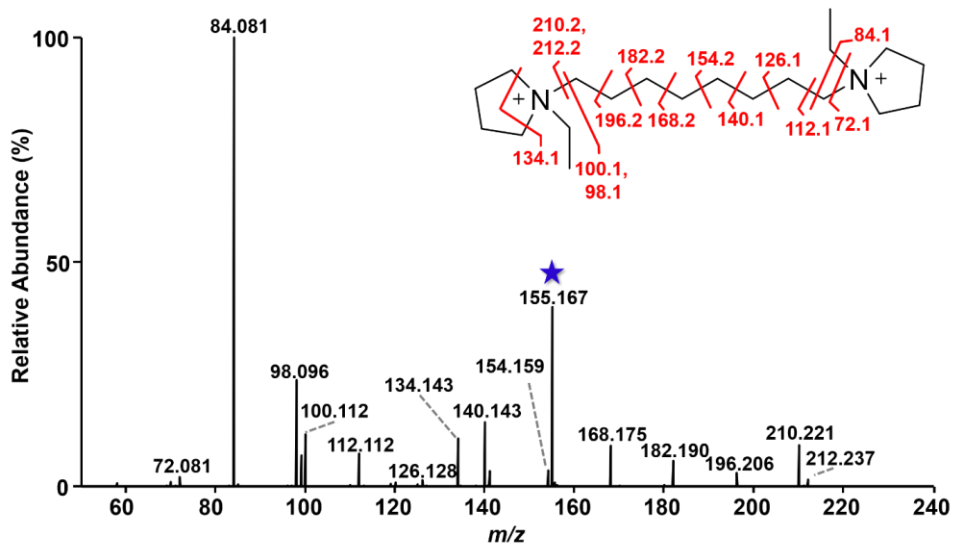


Figure S2. HCD fragmentation spectrum of the 1,8-ethyl dication used throughout this manuscript, illustrating successful synthesis of this product due to high mass accuracy of fragment ions and identification of all major fragment peaks within the spectrum. Selected precursor ions are designated with a star.

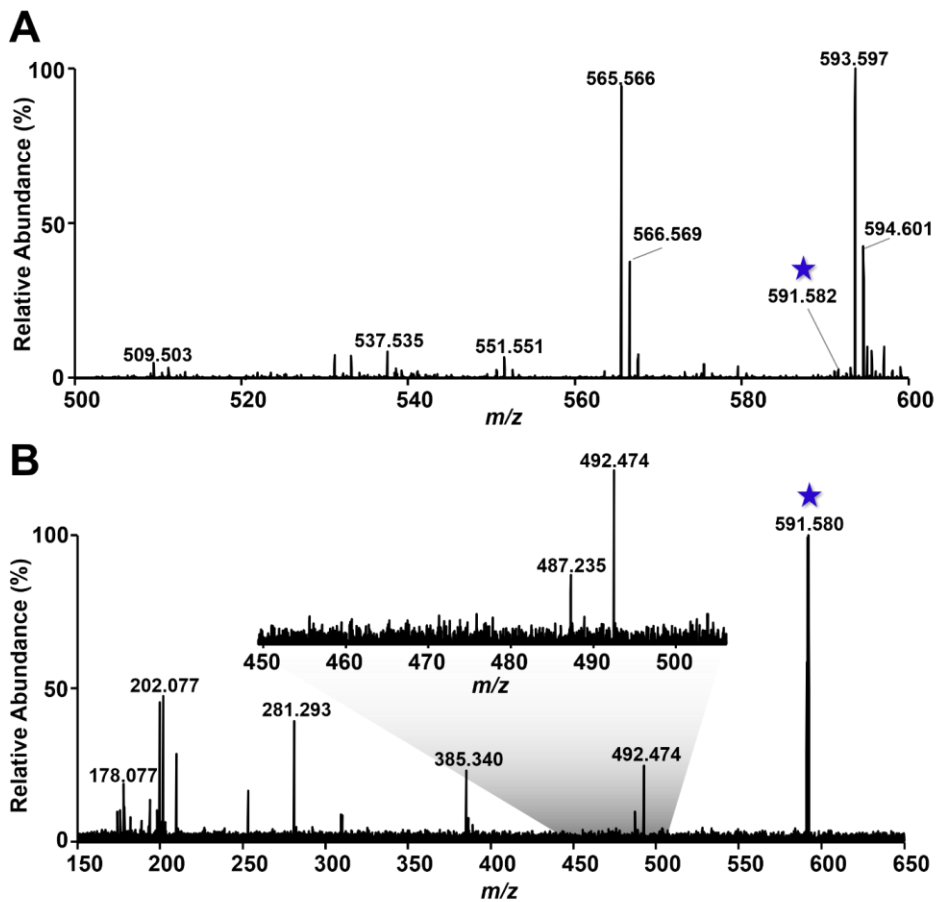


Figure S3. DESI-UVPD-MS spectrum from background signal of the DESI spray solvent on the glass slide (A) Full MS analysis of a glass slide, showing very low abundance (NL $\approx 4E3$) of m/z 591.582 compared to what is to be detected on the tissue section (NL $\approx 1E6$) (B) DESI-UVPD MS fragmentation of m/z 591.582 on a glass slide, showing no distinguishable peaks corresponding to the expected diagnostic fragment ions for FA 18:1 9 Δ or 11 Δ .

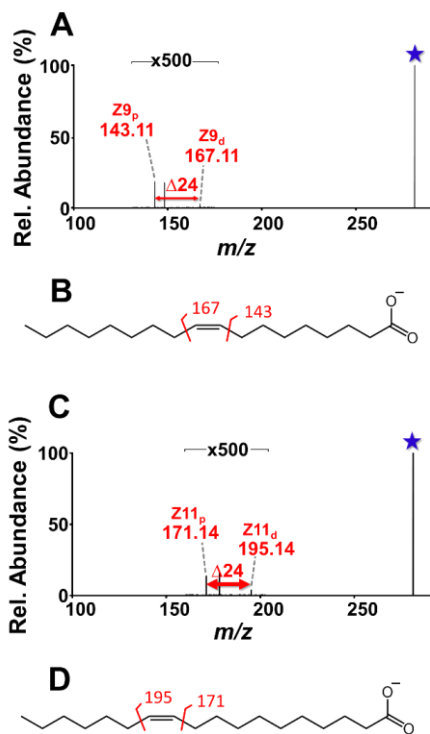


Figure S4. 193 nm UVPD (20 pulses, 4 mJ) spectra of deprotonated isomeric FA 18:1 structures (m/z 281.25). (A) UVPD spectrum of deprotonated FA 18:1(9Z) and (B) fragment map. (C) UVPD spectrum of deprotonated FA 18:1(11Z) and (D) fragment map. Selected precursor ions are designated with a star.

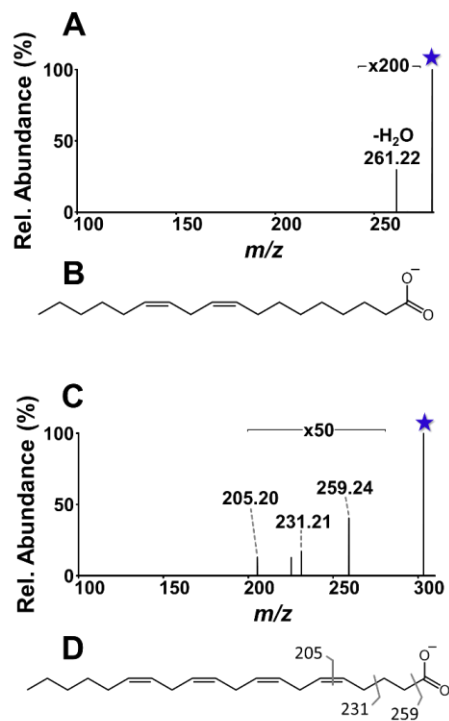


Figure S5. 193 nm UVPD (20 pulses, 4 mJ) spectra of deprotonated polyunsaturated FA structures. (A) UVPD spectrum of deprotonated FA 18:2(9Z,12Z) (m/z 279.23) and (B) structure. (C) UVPD spectrum of deprotonated FA 20:4(5Z,8Z,11Z,14Z) and (D) fragment map. Selected precursor ions are designated with a star.

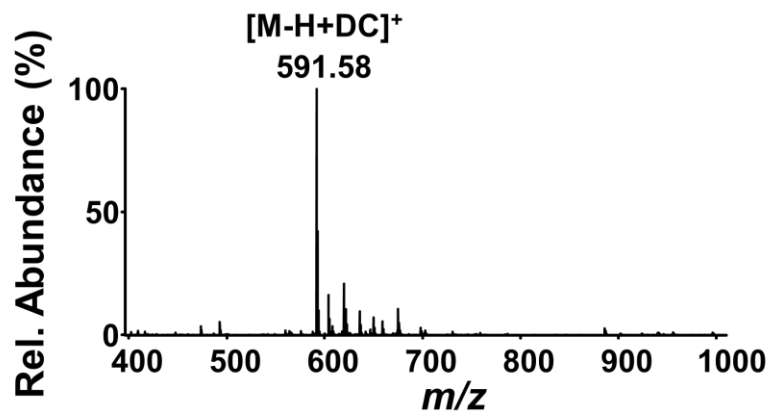


Figure S6. Positive mode MS1 spectrum of FA 18:1(9Z) complexed to 1,8-ethyl dication. MS² HCD and UVPD mass spectra for *m/z* 591.58 are shown in **Figure S5** and **1A**, respectively.

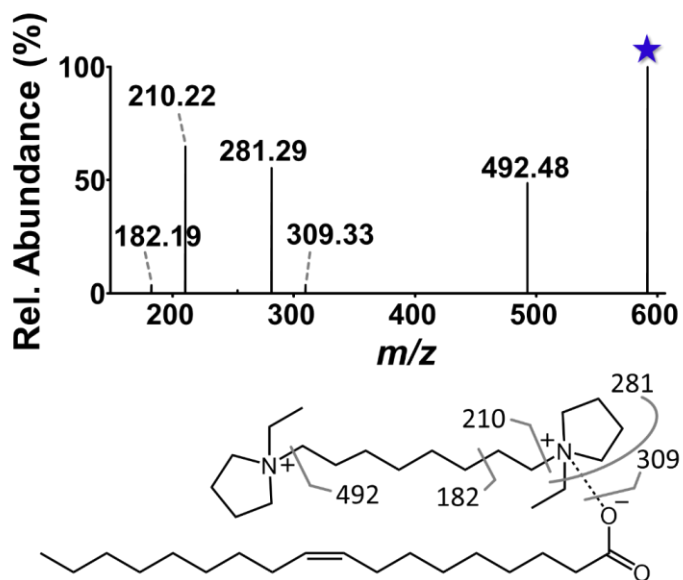


Figure S7. HCD (40 NCE) mass spectrum of FA 18:1(9Z) complexed to 1,8-ethyl dication (m/z 591.58) and corresponding fragment map. Selected precursor ion is designated with a star.

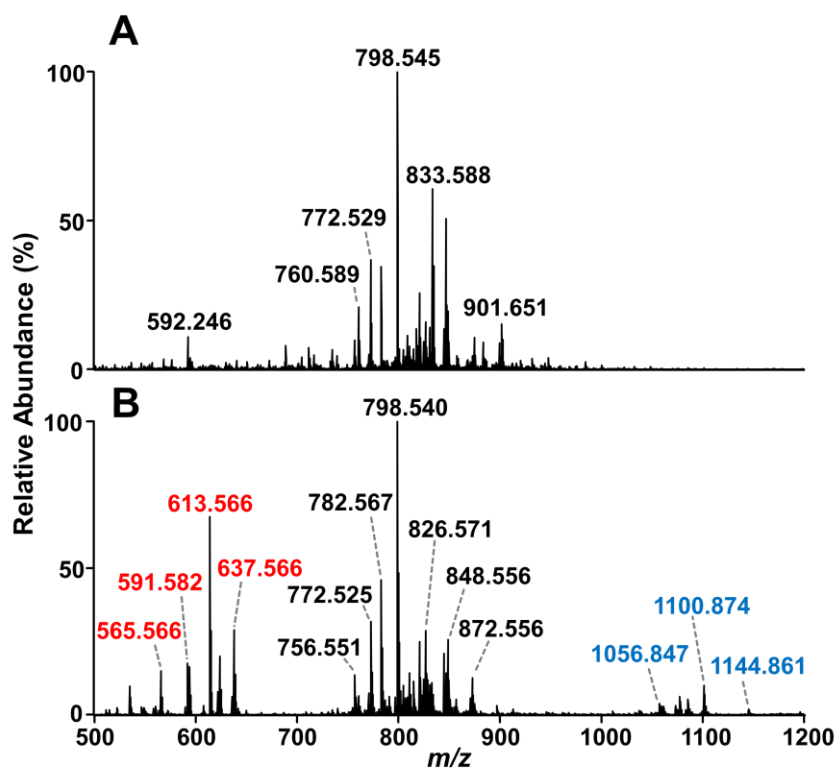


Figure S8. Full MS profile of mouse brain tissue analyzed by DESI-MS in the positive ion mode (A) without and (B) with the DC reagent added to the solvent. Peaks labeled in red are FA-DC complexes while peaks labeled in blue are glycerolphosphoethanolamine-DC complexes.

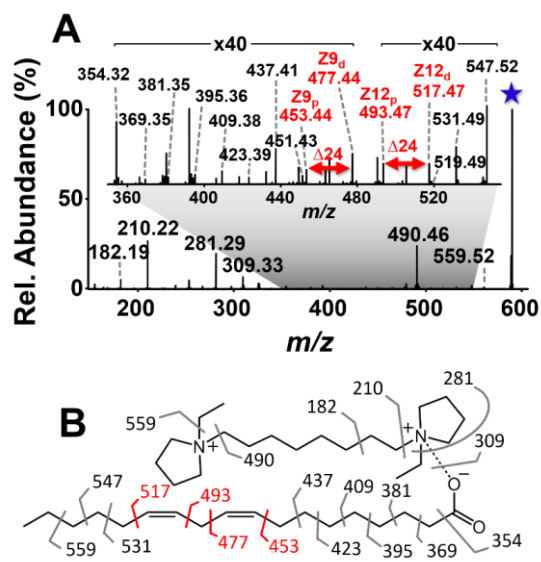


Figure S9. (A) 193 nm UVPD (20 pulses, 4 mJ) spectra for FA 18:2(9Z,12Z) complexed to 1,8-ethyl dication (m/z 589.57) and (B) corresponding fragment map. Pairs of diagnostic ions that localize the double bonds are highlighted. An expanded region of the spectrum with FA dissociation products is displayed in the inset. Selected precursor ion is designated with a star.

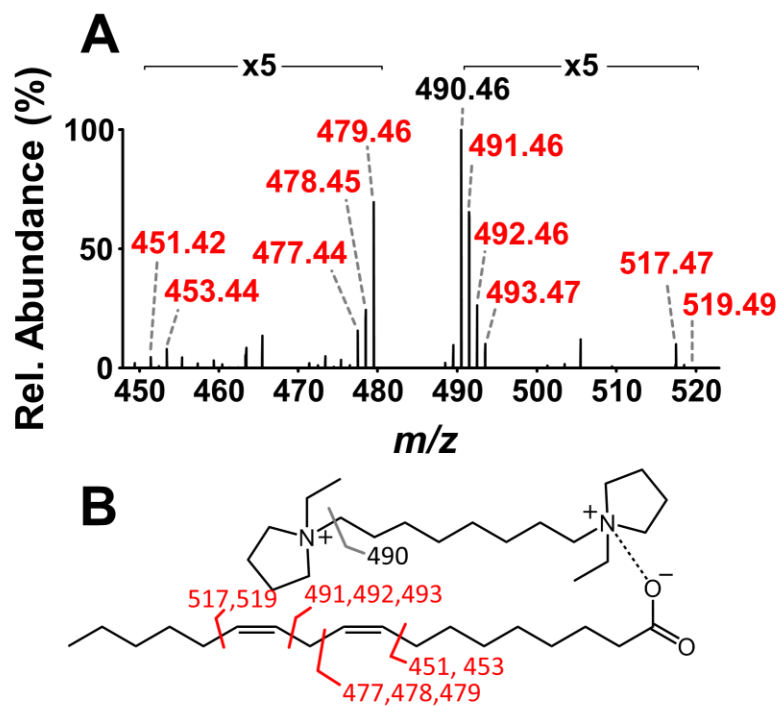


Figure S10. (A) Expanded region view of **Figure S7A**, displaying multiple products associated with cleavage of each C-C bond adjacent to a double bond. (B) Product m/z values were mapped to the FA structure.

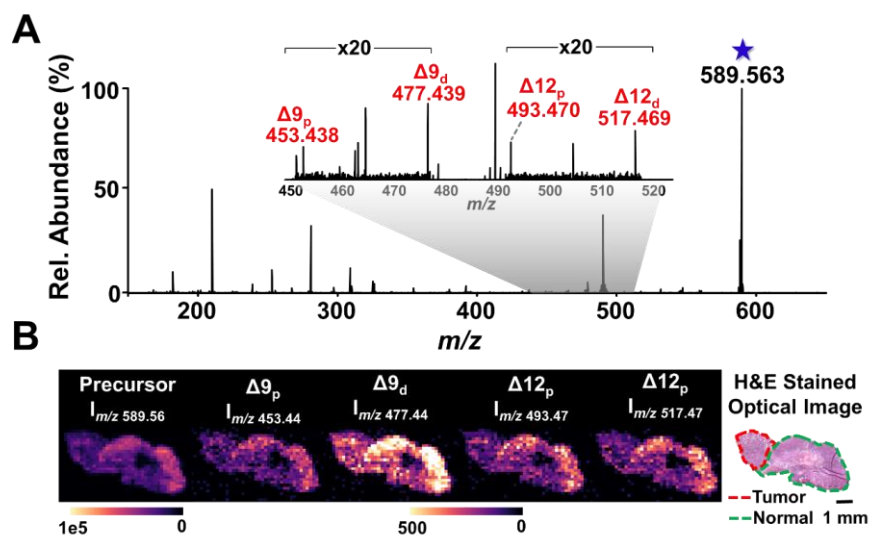


Figure S11. (A) DESI-UVPD mass spectrum from the fragmentation of FA18:2 precursor ion of m/z 589.56 from an ovarian tissue section (B) Ion images of the precursor and double bond diagnostic peaks, showing the distribution of the isomers within the ovarian tumor tissue section.

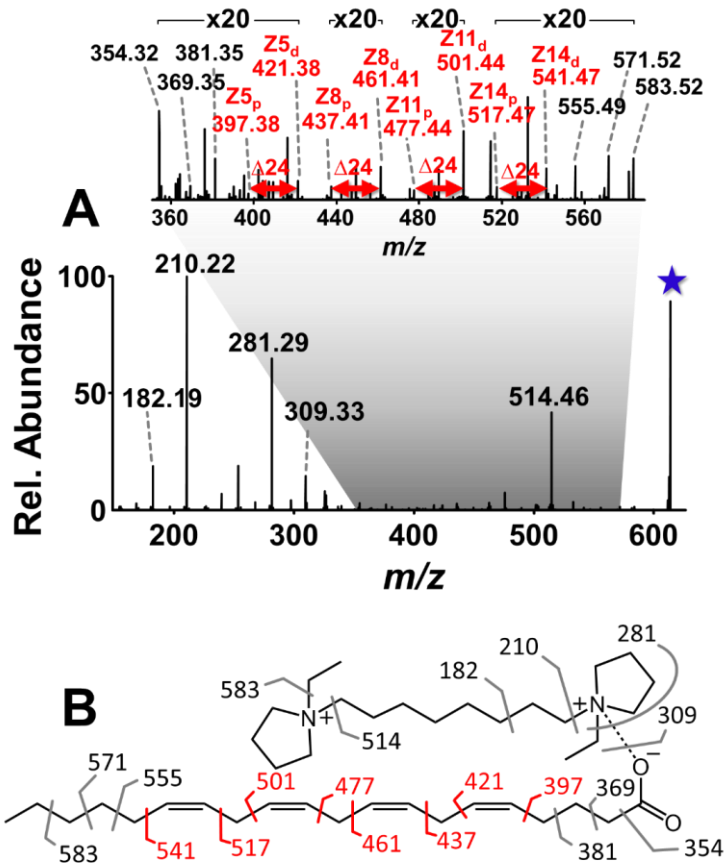


Figure S12. 193 nm UVPD (20 pulses, 4 mJ) mass spectra for FA 20:4(5Z,8Z,11Z,14Z) complexed to 1,8-ethyl dication (m/z 613.57) and (B) corresponding fragment map. Pairs of diagnostic ions that localize the double bonds are highlighted. An expanded region of the spectrum with FA dissociation products is displayed in the inset. Selected precursor ion is designated with a star.

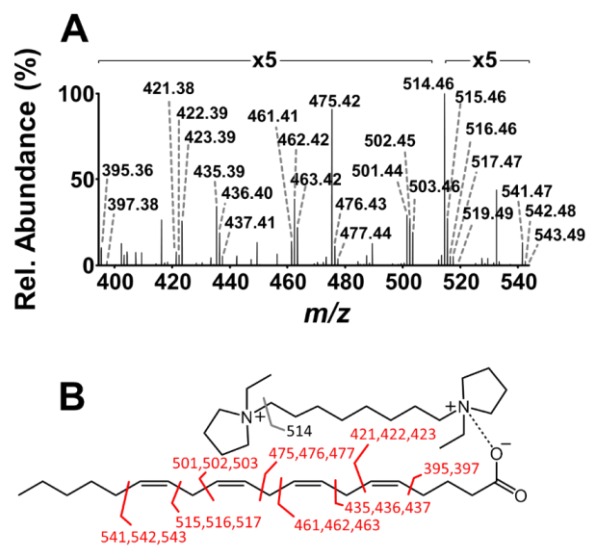


Figure S13. (A) Expanded region view of **Figure S12A**, displaying multiple products associated with cleavage of each C-C bond adjacent to a double bond. (B) Product m/z values were mapped to the FA structure.

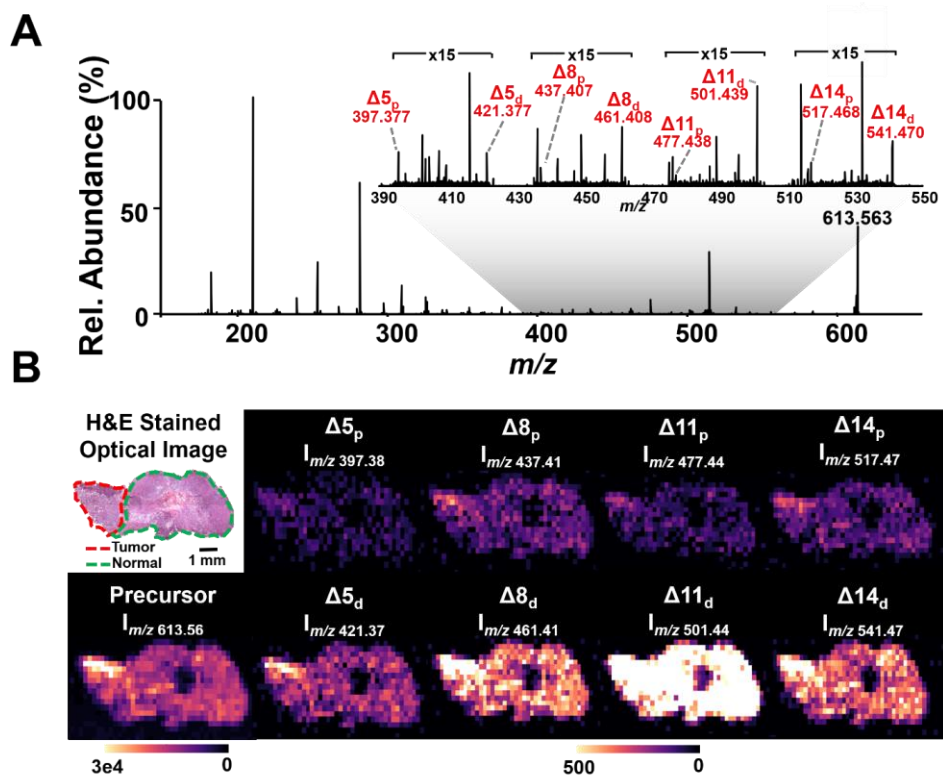


Figure S14. (A) DESI-UVPD mass spectrum from the fragmentation of FA 20:4 precursor at m/z 613.56 from an ovarian tissue section (B) Ion images of the precursor and select double bond diagnostic peaks, showing the distribution of the isomers within the ovarian tumor tissue section.

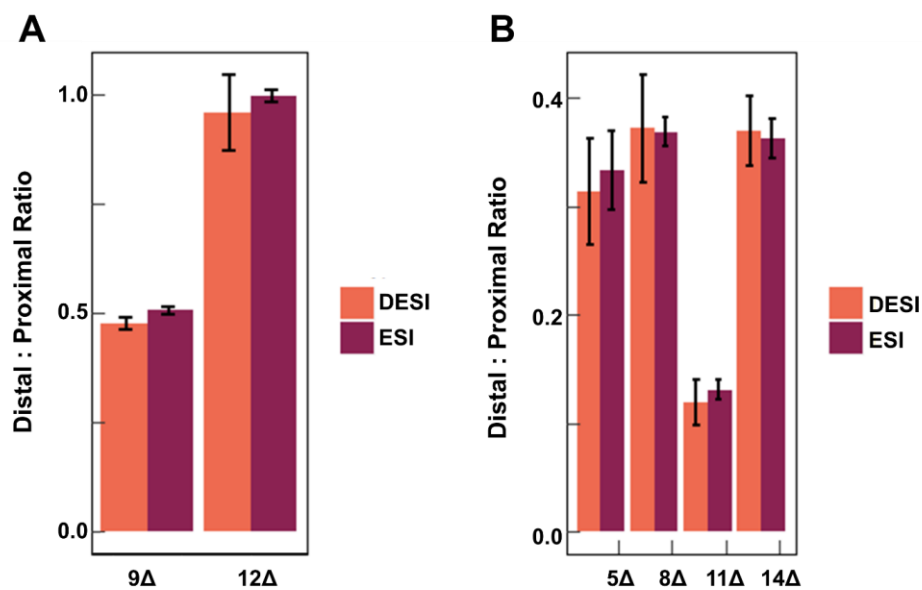


Figure S15. Comparison of distal:proximal fragment ion abundance ratios for each double bond for DC complexed (A) FA 18:2(9Z,12Z) and (B) FA 20:4(5Z,8Z,11Z,14Z) analyzed using FA standards in an ESI workflow and from ovarian tumor sections via reactive DESI, as discussed in the section *Strategy for determination of interfering fragments during DESI-MS imaging experiments* on page S6. Error bars are constructed from three separate ESI analyses and 3 DESI “lines” from one biological tissue section.

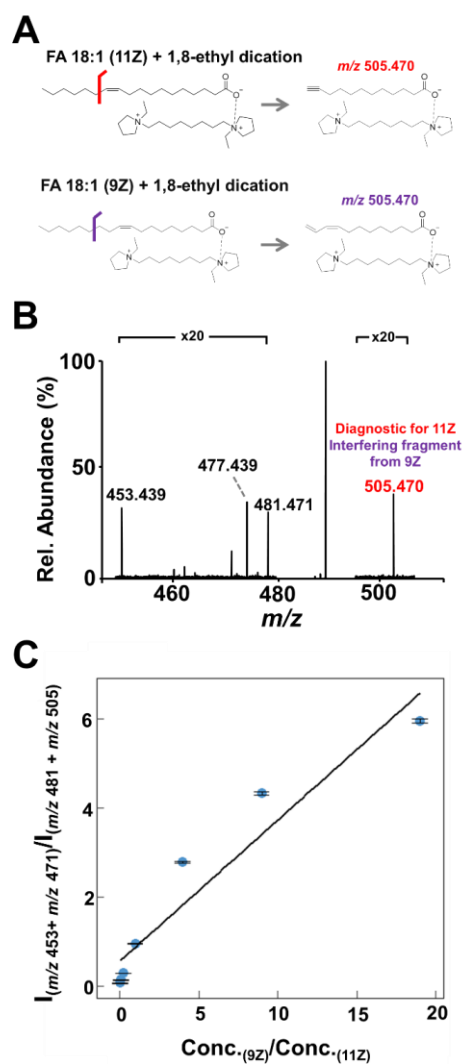


Figure S16. (A) Illustration of isomeric fragment ion structures that preclude the use of m/z 505 as a diagnostic product for quantitative analyses of double bond location in DC - FA 18:1 complex. (B) Representative UVPD mass spectrum for DC•FA 18:1 complex arising from a mixture of FA 18:1(9Z) and FA 18:1(11Z) standards, highlighting the m/z 505 product composed of interfering signals from the two isomers. (C) Calibration curve built from the ratio of the sum diagnostic ion intensities ($I_{(m/z\ 453+ m/z\ 471)} / I_{(m/z\ 481 + m/z\ 505)}$) versus concentration ratio of FA 18:1(9Z) to FA 18:1(11Z) ($\text{Conc.}_{(9Z)} / \text{Conc.}_{(11Z)}$) displays poor linearity.

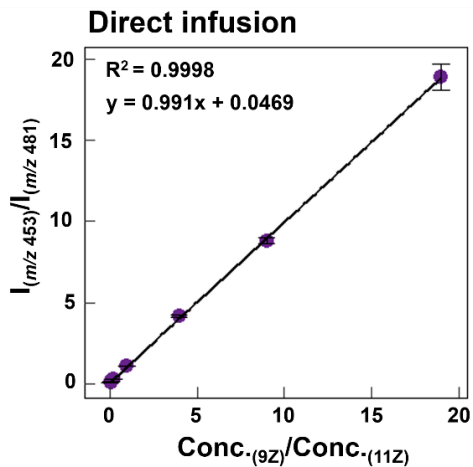


Figure S17. DC•FA 18:1 complexes were generated at varying FA 18:1(9Z)/FA 18:1(11Z) ratios and analyzed by UVPD in an ESI workflow. A linear relationship is demonstrated for the intensity ratio of the diagnostic ions ($I_{(m/z\ 453)}/I_{(m/z\ 481)}$) as a function of the concentration ratio of FA 18:1(9Z) to FA 18:1(11Z) ($\text{Conc.}_{(9Z)}/\text{Conc.}_{(11Z)}$).

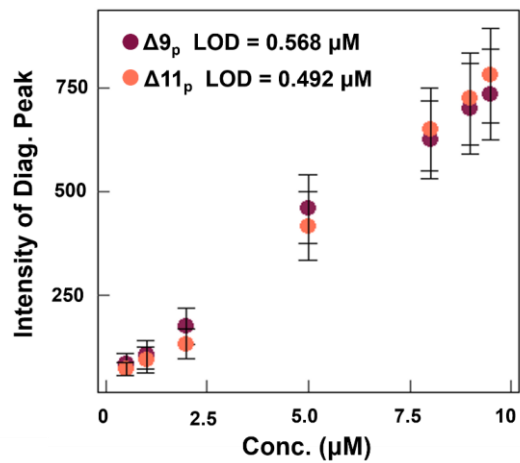


Figure S18: Calibration curves for the 9Z and 11Z proximal ions to determine limits of detection for reliable relative quantification of FA isomers during DESI-UVPD-MS. Each concentration ratio point is comprised of the average 9Z_p:11Z_p ratio where each technical replicate is one pixel from the spot shown in A, approximately 100 pixels per spot.

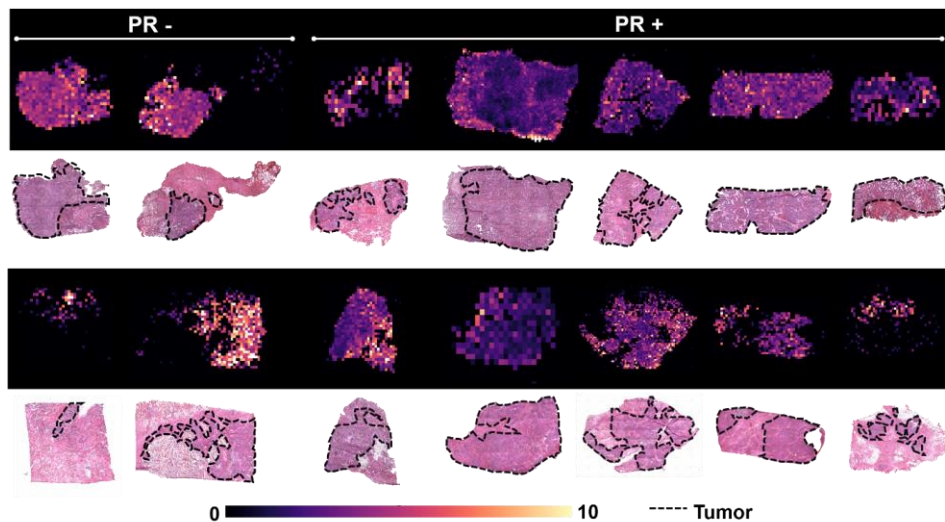


Figure S19: All DESI-UVPD MS images from PR- and PR+ samples. Tumor regions are outlined in black, with surrounding regions comprised of breast stroma, necrosis, lymphocytes, and other histological tissue types.

Supporting references:

- (1) Anderson, J. L.; Ding, R.; Ellern, A.; Armstrong, D. W. *Journal of the American Chemical Society* **2005**, *127*, 593-604.
- (2) Rao, W.; Mitchell, D.; Licence, P.; Barrett, D. A. *Rapid Communications in Mass Spectrometry* **2014**, *28*, 616-624.
- (3) Lostun, D.; Perez, C. J.; Licence, P.; Barrett, D. A.; Ifa, D. R. *Analytical Chemistry* **2015**, *87*, 3286-3293.
- (4) Kessner, D.; Chambers, M.; Burke, R.; Agus, D.; Mallick, P. *Bioinformatics* **2008**, *24*, 2534-2536.
- (5) Race, A. M.; Styles, I. B.; Bunch, J. *Journal of Proteomics* **2012**, *75*, 5111-5112.
- (6) Bokhart, M. T.; Nazari, M.; Garrard, K. P.; Muddiman, D. C. *Journal of The American Society for Mass Spectrometry* **2018**, *29*, 8-16.
- (7) Klein, D. R.; Brodbelt, J. S. *Analytical Chemistry* **2017**, *89*, 1516-1522.